1 **In situ chemical measurement of individual cloud residue particles at a**

2 **mountain site, South China**

3 Qinhao Lin[1,2], Guohua Zhang[1], Long Peng[1,2], Xinhui Bi[1,*], Xinming Wang[1], Fred J.

4 Brechtel[3], Mei Li[4], Duohong Chen[5], Ping'an Peng[1], Guoying Sheng[1], Zhen Zhou[4]

6 [1] State Key Laboratory of Organic Geochemistry and Guangdong Key Laboratory of

7 Environmental Protection and Resources Utilization, Guangzhou Institute of Geochemistry,

8 Chinese Academy of Sciences, Guangzhou, 510640, PR China

9 [2] University of Chinese Academy of Sciences, Beijing, 100049, PR China

10 [3] Brechtel Manufacturing Inc., Hayward, 94544, California, USA

11 [4] Atmospheric Environment Institute of Safety and Pollution Control, Jinan University,

12 Guangzhou 510632, PR China

13 [5] State Environmental Protection Key Laboratory of Regional Air Quality Monitoring,

14 Guangdong Environmental Monitoring Center, Guangzhou 510308, PR China

16 * Correspondence to: Xinhui Bi (bixh@gig.ac.cn)

17 Tel.: +86-20-85290195

Highlights

1. EC-containing particles comprised the largest fraction of cloud residues (49.3% by number).

2. Amine particles represented 0.2% to 15.1% by number of the cloud residues dependent on the air mass history.

3. Nitrate intensity increased in the cloud residues relative to the ambient particles but decreased compared with interstitial particles.

4. Sulfate intensity increased in the aged EC and OC cloud residues and decreased in the dust and Na-rich cloud residues.

28   **Abstract**

29   To estimate how atmospheric aerosol particles respond to chemical properties of cloud

30   droplets, a ground-based counterflow virtual impactor (GCVI) coupled with a real-time

31   single-particle aerosol mass spectrometer (SPAMS) was used to assess the chemical

32   composition and mixing state of individual cloud residue particles in the Nanling Mountain

33   Range (1,690 m a.s.l.), South China, in January 2016. The cloud residues were classified

34   into nine particle types: Aged elemental carbon (EC), Potassium-rich (K-rich), Amine,

35   Dust, Pb, Fe, Organic carbon (OC), Sodium-rich (Na-rich) and Other. The largest fraction

36   of the cloud residues was the aged EC type (49.3% by number), followed by the K-rich

37   type (33.9% by number). Abundant aged EC cloud residues that internally mixed with

38   inorganic salts were found in air masses from northerly polluted areas. The number fraction

39   (Nf) of the K-rich cloud residues significantly increased within southwesterly air masses

40   from fire activities in Southeast Asia. In addition, the Amine particles represented 0.2% to

41   15.1% by number to the cloud residues when air masses changed from northerly to

42   southwesterly sources. The Dust, Fe, Pb, Na-rich and OC particles had a low contribution

43   (0.5-4.1% by number) to the cloud residues. An analysis of the mixing state of cloud

44   residues showed that the Dust and Na-rich cloud residues were highly associated with

45   nitrate. Sulfate intensity increased in the aged EC and OC cloud residues and decreased in

46   the Dust and Na-rich cloud residues relative to both ambient and interstitial particles. A

47   comparison of cloud residues with interstitial particles indicated that a higher Nf for K-rich

48   particles and a lower Nf for the aged EC particles were found in the cloud residues. Relative

49   to the ambient and interstitial particles, the cloud residues exhibited larger size distributions.

50   To our knowledge, this study is the first report on in situ observation of the chemical

51   composition and mixing state of individual cloud residue particles in China. This study

52   increases our understanding of the impacts of aerosols on cloud droplets in a remote area

53   of China.

54

55   Keywords: GCVI, SPAMS, cloud residues, mixing state, South China

56

57

58   **1 Introduction**

59   Aerosol-cloud interaction influences the thermodynamic and radiation balance of the

60   atmosphere (IPCC, Boucher et al., 2013). Atmospheric aerosol particles can act as cloud

61   condensation nuclei (CCN) and subsequently affect the chemical and physical properties

62   of cloud droplets, which in turn influence global and regional climate change. The ability

63   of atmospheric aerosol particles to act as CCN, particularly in terms of temporal and spatial

64   variation, may usefully improve estimates of climate change. Anthropogenic particles have

65   been observed to be enriched in the cloud droplets at Schmücke (Roth et al., 2016).

66   However, a lesser abundance of anthropogenic particles was found in the mixed-phase

67   clouds during the Cloud and Aerosol Characterization Experiment (CLACE 6) (Kamphus

68   et al., 2010). Therefore, it is crucial to assess how atmospheric aerosol particles contribute

69   and respond to the chemical composition of cloud droplets in different regions.

70   The formation of CCN is dependent on the size and chemical composition of

71   atmospheric aerosol particles at a given supersaturation (McFiggans et al., 2006). A change

72   in the chemical composition of atmospheric aerosol particles during atmospheric aging

73   processes can strongly alter their CCN ability. The presence of hydrophobic surface films

74   lowers the CCN ability of atmospheric aerosols (Andreae and Rosenfeld, 2008). Elemental

75   carbon (EC) particles, normally considered insoluble, show high CCN activity after mixing

76   with sulfuric acid (Zhang et al., 2008). However, sulfate and nitrate, which are generally

77   regarded as soluble materials, were found in particles ranging from high to low

78   hygroscopicity (Herich et al., 2008). Furthermore, several cloud measurements have

79   pointed to a lower Nf of sulfate in cloud droplets relative to ambient or interstitial particles

80   (Twohy and Anderson, 2008; Pratt et al., 2010a). On the contrary, other study have reported

81   a larger Nf of sulfate in cloud droplets (Roth et al., 2016). These discrepancies suggest that

82   the influence of the mixing state of atmospheric aerosol particles on CCN activity remains

83   unclear.

84   The combined technique of a counterflow virtual impactor (CVI) and Aerosol Mass

85   Spectrometer (AMS) or single-particle measurement is widely used to characterize the

86   chemical composition and mixing state of individual cloud/fog droplet residue particles.

87   These studies mainly focus on Europe (Drewnick et al., 2007; Kamphus et al., 2010; Roth

88   et al., 2016; Schneider et al., 2016) and North America (Hayden et al., 2008; Berg et al.,

89   2009; Pratt et al., 2010b; Zelenyuk et al., 2010). Over the past three decades, China has

90   undergone rapid economic growth accompanied by increased aerosol emissions. Scientists

91   have worked to increase our understanding of an emissions inventory and the temporal and

92   spatial variation of atmospheric aerosols in China (Zhang et al., 2012b). However, few

93   studies employ direct observation of the chemical composition and mixing state of

94   cloud/fog droplets. Bi *et al.* (2016) used a ground-counterflow virtual impactor (GCVI)

95   coupled with a real-time single particle aerosol mass spectrometer (SPAMS) to explore the

96   chemical composition and mixing state of single fog residue particles in an urban area of

97   South China at ground level. They found abundant anthropogenic emitted particles

98   including soot or element carbon (EC) in fog droplets. Here, we present a study on the

99   chemical composition and mixing state of individual cloud residue particles at a mountain

100   site. The same experimental methods of Bi et al. (2016) were used in this study on the

101   summit of South China's Nanling mountain region. The size distribution, chemical

102   composition and mixing state of cloud residues during cloud events are discussed.

103   Moreover, the chemical compositions of ambient and interstitial particles were also

104   compared with the cloud residues. The aim of this study is to assess the potential effects of

105   anthropogenic aerosols from regional transportation on cloud formation and to investigate

106   the dominant particle types in cloud droplets at a mountain site in South China.

107

108   **2 Experimental**

109   **2.1 Measurement site**

110   Measurements were carried out January 15-26, 2016. The sampling site was located in the

111   Nanling Background Station (112° 53' 56" E, 24° 41' 56" N, 1,690 m a.s.l.) at the National

112   Air Pollution Monitoring System in South China (Figure S1). This station is 200 km north

113   of the metropolitan city Guangzhou and 350 km north of the South China Sea. This site is

114   also surrounded by a national park forest (273 km^2) where there are hardly any emissions

115   from anthropogenic activities. However, during the winter monsoon period, air pollution

116   from northern China moves south to the southern coastal region and crosses the study

117   region (Lee et al., 2005).

118

119   **2.2 Instrumentation**

120   In this study, a GCVI inlet system (GCVI Model 1205, Brechtel Mfg. Inc.) was used to

121   sample cloud droplets with a diameter greater than 8 µm. The sampled cloud droplets were

122   passed through an evaporation chamber (air flow temperature at 40 °C), where the

123   associated water was removed and the dry residue particles, considered CCN, remained.

124   The particle transmission efficiency of the cut size (8 µm) was 50% (Shingler et al., 2012).

125   The enrichment factor of the particles collected by the GCVI inlet was estimated to be 5.25

126   based on theoretical calculation (Shingler et al., 2012). Ambient particles were collected

127   through an ambient inlet with a cut-off aerodynamic diameter (d_{va}) of 2.5 µm when no

128   cloud events were present. Additionally, interstitial particles were sampled through the

129   ambient inlet during cloud events. The cloud droplet residues, interstitial particles or

130   ambient particles were subsequently analyzed by a suite of aerosol measurement devices,

131   including a SPAMS (Hexin Analytical Instrument Co., Ltd., Guangzhou, China), a

132   scanning mobility particle sizer (SMPS) (MSP Cooperation) and an aethalometer (AE-33,

133   Magee Scientific Inc.). Detailed information and parameter settings regarding the GCVI

134   operation can be found in the work of Bi et al. (2016). Previous studies have found that the

135   average size of cloud droplets in this region was approximately 10 µm, with a

136   corresponding liquid water content of 0.11-0.15 g m^{-3} (Deng et al., 2007). Therefore, it is

137   reasonable to assume that particles larger than 8 µm are cloud droplets. Here, we focus on

138   in situ observations of the size-resolved chemical composition and the mixing state of

139   single cloud residue particles measured by the SPAMS. Meteorological parameters and

140   PM$_{2.5}$ values at this site were provided by Guangdong Environmental Monitoring Center.

141   A detailed operational principle of the SPAMS has been described elsewhere (Li et al.,

142   2011). Briefly, aerosol particles are drawn into SPAMS through a critical orifice. The

143   particles are focused and aerodynamically sized by two continuous diode Nd:YAG laser

144   beams (532 nm). The particles are subsequently desorbed/ionized by a pulsed laser (266

145   nm) triggered exactly based on the velocity of the specific particle. The positive and

146   negative ions generated are recorded with the corresponding size of each singe particle.

147   The velocity is related to vacuum d_{va} using a calibration curve created from the measured

148   velocities of a series of polystyrene latex spheres (Nanosphere Size Standards, Duke

149   Scientific Corp., Palo Alto) with predefined sizes. Particles measured by SPAMS mostly

150   fell within the size range of d_{va} 0.2-2.0 μm (Li et al., 2011). This makes it impossible to

151   effectively detect particles that exceed such a size range (Figure S2).

152

153   **2.3 Definition of cloud events**

154   To reliably identify the presence of cloud events, an upper-limit visibility threshold of 5

155   km and a lower-limit relative humidity (RH) threshold of 95% were set in the GCVI

156   software (Bi et al., 2016). Three long-time cloud events occurred during the periods of

157   16:00 (local time) 15 January - 07:00 17 January (cloud I), 20:00 18 January - 12:00 19

158   January (cloud II) and 17:00 19 January - 13:00 23 January (cloud III), as marked in Figure

159   1. In addition, a cloud event occurred during 14:40 - 15:00 17 January, but we did not

160   complete an analysis due to the short duration of this cloud event. The average values of

161   cloud droplet concentrations integrated by the SMPS were 218 cm^{-3}, 284 cm^{-3} and 272

162   cm^{-3} for cloud I, cloud II and cloud III, respectively (Figure S2). Note that during cloud

163   events, RH was close to 100%, as illustrated in Figure 1. Hazy days associated with low

164   visibility were almost completely excluded in this study due to the low level of PM$_{2.5}$ (~

165   12.7 μg m^{-3}). A rainfall detector of the GCVI system was also used to exclude rainy droplet

166   contamination. When cloud events occurred without precipitation, sampling was

167   automatically triggered by the GCVI control software.

168

169   **2.4 Particle classification**

170   During the study period, a total of 73996 sampled particles including 49322 ambient, 23611

171   cloud residues and 1063 interstitial particles with bipolar mass spectra were chemically

172   analyzed in the size range of d_{va} 0.2-1.9 μm.   The sampled particles were first classified

173   into 101 clusters using an Adaptive Resonance Theory neural network (ART-2a) with a

174   vigilance factor of 0.75, a learning rate of 0.05, and 20 iterations (Song et al., 1999). By

175   manually combining similar clusters, aged EC, Potassium-rich (K-rich), Amine, Dust, Fe,

176   Pb, Organic carbon (OC), and Sodium-rich (Na-rich), eight major particle types with

177   distinct chemical patterns were obtained, which represented ~99.9% of the population of

178   the detected particles. The remaining particles were grouped together as "Other".

179   Assuming that number of individual particles follows Poisson distribution, standard errors

180   for number fraction of particle type were estimated (Pratt et al., 2010a).

181

182   **3 Results and discussion**

183   **3.1 Back trajectories and meteorological conditions**

184   Back air trajectories in this study were calculated using the Hybrid Single Particle

185   Lagrangian Integrated Trajectory (HYSPLIT Model). During the study period, the station

186   was mainly affected by southwesterly or northerly air masses (Figure 2). The southwesterly

187   air masses, accompanied by warm and moist airflows, occurred during 15-17 and 19-22

188   January, which promoted cloud formation (Figure 1). Conversely, the northerly air masses,

189   associated with cool and dry airstreams, occurred during 18 and 23-26 January and led to

190   a decrease in temperature and relative humidity. Meteorological conditions were unstable,

191   with high southwesterly flow (~ 6.5 m s^{-1}) during 15-17 and 20-22 January (Figure 1). The

192   level of PM$_{2.5}$ remained low with a value of approximately 3 μg m^{-3} for this time period.

193   A high level of PM$_{2.5}$ ($\sim$20 μg m^{-3}) was observed during 18 January when the northerly

194   flow dominated. Similarly, the average PM$_{2.5}$ value reached 24 μg m^{-3} during 24-26

195   January when the local northerly and southwesterly flows occurred alternately. However,

196   the particles still originated from northerly air masses for this period (Figure 2). During 23-

197   24 January, a big freeze associated with a violent northerly flow and a wind speed that

198   exceeded the upper-limit speed ($\sim$12 m/s) of a wind speed sensor resulted in a sharp

199   decrease in temperature (Figure 1).

200

201   **3.2 The chemical characterization of cloud droplet residues**

202   Figure 3 shows the average positive and negative mass spectra of nine particle types. The

203   aged EC particles were identified by EC cluster ions (e.g., m/z $\pm12C^{+/-}$, $\pm36C_3^{+/-}$, $\pm48C_4^{+/-}$,

204   $\pm60C_5^{+/-}$, …) and a strong sulfate ion signal (m/z -97HSO$_4^-$) and some organic markers

205   (m/z 27, 37). The aged EC particle type was the largest fraction (49.3% by number) of the

206   cloud residues (Figure 4). In addition, the number fraction (Nf) of aged EC particles in the

207   cloud residues significantly decreased while size increased (Figure S3). The K-rich

208   particles exhibited the highest peak at m/z 39K$^+$, mainly combined with sulfate and nitrate

209   (m/z -46NO$_2^-$, -62NO$_3^-$). The K-rich particles presumably resulted from biomass/biofuel

210   burning (Moffet et al., 2008; Zhang et al., 2013). The K-rich particle type, the second

211   largest contributor, accounted for 33.9% by number of the cloud residues (Figure 4). Aged

212   EC and K-rich particles mainly originated from combustion processes (Andreae and

213   Rosenfeld 2008; Bond et al., 2013). The Nanling mountain sampling site does not contain

214   any sources of anthropogenic emissions; thus, the abundant aged EC and K-rich particles

215   in cloud residues are expected to come from regional transportation.

216   The Amine particles were characterized by related amine ion signals at m/z

217   $58C_2H_5NHCH_2^+$, $59N(CH_3)_3^+$ (trimethylamine, TMA) and $86C_5H_{12}N^+$ (Angelino et al.,

218   2001;Moffet et al., 2008;Pratt and Prather, 2010). This particle type also contained sulfuric

219   acid ion signals at m/z $-195H(HSO_4)_2^-$, indicative of acidic particles (Rehbein et al., 2011).

220   The Amine particles represented 3.8% by number of the cloud residues (Figure 4), mainly

221   within the size fraction of 0.7-1.9 µm (Figure S3). A recent study also showed a low

222   fraction (<10% by number) of amine species in the cloud residues (Roth et al., 2016). It

223   has been reported that in-cloud/fog processing could enhance amine species (Rehbein et

224   al., 2011; Zhang et al., 2012a). However, this possibility was not supported by the

225   observations of Bi et al. (2016), who did not detect amine-containing particles in the fog

226   residues. In this study, the Nf of the Amine particles varied from 0.2% to 15.1% of the

227   cloud residues dependent on air mass history (see Sect. 3.4).

228   The Dust particles presented significant ions at m/z $40Ca^+$, $56CaO^+/Fe^+$, $96Ca_2O^+$ and -

229   $76SiO_3^-$, with an internal mixture of sulfate and nitrate. This type contributed 2.9% by

230   number of the cloud residues (Figure 4). Dust/mineral aerosol accounted for approximately

231   35% of the total aerosol mass in China (Zhang et al., 2012b). Approximately 12% by

232   number of fog contained dust particles at ground level in South China (Bi et al., 2016). At

233   Mt. Taishan in northern China, a high concentration of Ca^{2+} in cloud/fog water was mainly

234   attributed to a sandstorm event (Wang et al., 2011). In this study, a low fraction (2.9% by

235   number) of dust cloud residue suggests that dust particles did not play a significant role in

236   cloud formation in South China or that they occupied larger CCN (Tang et al., 2016), which

237   cannot be detected by the SPAMS.

238   The Fe and Pb particles had their typical ions at m/z $56Fe^+$ and $208Pb^+$, respectively, and

239   were associated with sulfate and nitrate. The Fe and Pb particles made up 4.1% and 0.5%

240   by number of the cloud residues, respectively (Figure 4). The presence of Fe in the cloud

241   droplets might play an important role in aqueous-phase SO_2 catalytic oxidation in cloud

242   processing (Harris et al., 2014), thus accelerating the sulfate content of Fe-containing

243   particles in cloud processing.

244   The Na-rich particles were mainly composed of ion peaks at m/z $23Na^+$ and $39K^+$ in the

245   positive mass spectra, and inorganic soluble nitrate and sulfate species in the negative mass

246   spectra. Moffet et al. (2008) attributed Na-rich particles to varied sources of industrial

247   emissions or sea salt particles and dry lake beds. The OC particles presented dominant

248   intense OC signals (e.g., m/z $27C_2H_3^+$, $37C_3H^+$, $43C_2H_3O^+$ and $51C_4H_3^+$) and abundant

249   sulfate. The Na-rich and OC types contributed 3.0% and 2.4% by number to the cloud

250   residues, respectively (Figure 4). Internally mixed EC with metal signatures was observed

251   in the Other particles. However, Other particles contributed only 0.1% by number to the

252   cloud residues, which suggests their minor contribution to cloud formation (Figure 4).

253

254   **3.3 Mixing state of secondary species in cloud residues**

255   Particles that coated with inorganic species (e.g., sulfate, nitrate and ammonium) can

256   facilitate water uptake to growth into cloud droplets (Andreae and Rosenfeld, 2008).

257   Number fractions of sulfate were found to be highly related to the K-rich (91%), OC

258   (100%), aged EC (98%), Pb (74%), Fe (93%) and Amine (99%) cloud residues, as shown

259   in Figure 5. Lower number fractions of sulfate were observed in the Na-rich (41%) and

260   Dust (42%) cloud residues. In contrast, nitrate contributed 89% and 88% by number to the

261   Na-rich and Dust cloud residues, respectively. The heterogeneous and/or aqueous

262   chemistry of HNO_3 in the Na-rich and dust particles may lead to the preferential enrichment

263   of nitrate (Li and Shao, 2009). The detection of nitrate in the cloud residues was thought

264   to be the form of ammonium nitrate by estimating the ratio of m/z 30 to m/z 46 in AMS

265   data (Drewnick et al., 2007; Hayden et al., 2008). However, low portions of ammonium in

266   the Na-rich (23% by number) and Dust (15% by number) cloud residues suggest that

267   ammonium nitrate is not a predominant form of nitrate in these cloud residue particle types.

268   Note that the evaporation chamber of the GCVI may lead to a reduction of ammonium

269   nitrate in the cloud residues (Hayden et al., 2008; Prabhakar et al., 2014). However, this

270   effect would be insignificant because the dry carrier air of the GCVI was set at 40 °C. A

271   volatility study found that the temperature to evaporate ammonium nitrate particles reached

272   at least 75 °C (Bi et al., 2015). We found that nitrate accounted for only 46% by number

273   of the aged EC cloud residues, which is significantly less than the contribution of sulfate.

274   Previous studies found that aged EC (soot) fog/cloud residues are mainly internally mixed

275   with sulfate (Pratt et al., 2010a; Harris et al., 2014; Bi et al., 2016). The presence of

276   abundant sulfate in aged EC cloud residues was considered to be a good CCN species

277   before activation, rather than formed by in-cloud processing (Bi et al., 2016; Roth et al.,

278   2016). High portions (75-86% by number) of ammonium were observed for the OC and

279   EC cloud residues, suggesting that ammonium plays a key role in cloud processes for the

280   two cloud residue types.

281   Organics (e.g., amine and oxalate) have previously been measured in cloud residues

282   (Sellegri et al., 2003; Sorooshian et al., 2007b; Pratt et al., 2010a). Amine and oxalate

283   particles with mixtures of inorganic salts could enhance water uptake behavior (Sorooshian

284   et al., 2008; Wu et al., 2011). Enrichment of TMA (93% by number) in the Amine cloud

285   residues is expected to promote water uptake in sub- and supersaturated regimes

286   (Sorooshian et al., 2007a). A total of 3,410 oxalate-containing (m/z, $-89 HC_2O_4^-$) particles

287   represented 14.4% of the cloud residues by number, which was mainly associated with the

288   K-rich cloud residues including 2,144 oxalate particles. The oxalate in the K-rich cloud

289   residues is likely attributed to biomass burning, which facilitates the CCN ability of

290   biomass-burning particles due to the hygroscopic property of oxalate (Pratt et al., 2010a).

291   Relative high portions (~30% by number) of oxalate in the metal (Pb, Fe) cloud residues

292   might be the form of metal oxalate complexes from reactions of in-cloud formation oxalate

293   with metals (Furukawa and Takahashi, 2011). Oxalate can readily partition into the particle

294   phase to form amine salts (Pratt et al., 2009). This may result in 33% by number to the

295   Amine residues containing oxalate.

296

297   **3.4 Comparison of cloud residues in different air mass sources**

298   Figure 6 displays hourly average unscaled counts and Nf values of nine types of cloud

299   residues and ambient particles. During 18-19 January, the cloud residues and ambient

300   particles showed similar chemical characteristics and were dominated by aged EC particles.

301   A lack of significant variation in the Nf of particle types for this period suggests that the

302   original particles did not change. Based on a backward trajectory, air masses changed from

303   northerly on 18 January to southwesterly on 19 January (Figure 2), consistent with variation

304   in local wind (Figure 1). Weak wind flow (~ 2.75 m s^{-1}) on 19 January favored the

305   accumulation of particles that originated from northerly air masses on 18 January, with a

306   remaining high level of PM$_{2.5}$ (~ 16 µg m^{-3}). During 16-17 and 21-22 January, the cloud

307   residues consisted of a high fraction of the Amine type, which significantly differed from

308   the observation during 18-19 January. Clearly, the observations during 16-17 and 21-22

309   January were influenced by a strong southwesterly flow with a low value of PM$_{2.5}$ (~ 3 µg

310   m^{-3}).

311   As mentioned above, the Nf of the cloud residue types significantly changed as the air

312   mass origin varied from northerly to southwesterly. To further investigate the influence of

313   air mass history, we selected cloud residues that had arrived from a northerly air mass on

314   19 January and compared these to cloud residues originating from a southwesterly air mass

315   during the periods of 16-17 and 21-22 January. The detected number of cloud residues for

316   the northerly and southwesterly air masses are given in Table 1. Note that southwesterly

317   air mass accompanied by high relative humidity (>90%) (Figure S4) may have triggered

318   particles activated to CCN prior to their arrival to the sampling site.

319   The K-rich type was found to contribute 23.9% to the cloud residues in the northerly air

320   mass, which was significantly lower than its contribution to the southwesterly air mass

321   (51.5%), as summarized in Table 1. The considerable increase of K-rich cloud residues

322   suggests a major influence of regional biomass-burning activities. Biomass-burning

323   emissions from Southeast Asia, including Myanmar, Vietnam, Laos and Thailand, where

324   abundant fire dots are observed (Figure 2), could have been transported to the sampling

325   site under a southwesterly air mass (Duncan et al., 2003). In contrast, the aged EC type

326   represented only 23.7% of the cloud residues under the influence of a southwesterly air

327   mass, which was significantly lower than observations for the northerly air mass (59.9%).

328   This result suggests that the northern air mass has a greater influence on the presence of

329   aged EC cloud residues.

330   In addition, an obvious increase in Nf of the Amine type was observed in the

331   southwesterly air mass (15.1%) compared to the northerly air mass (0.2%). This implies

332   that the sources or formation mechanisms of amine in cloud residues varied in different air

333   masses. The southwesterly air mass arrived from as far as the Bay of Bengal and then

334   travelled through Southeast Asia before reaching South China (Figure 2). The potential gas

335   amine emissions from ocean (Facchini et al., 2008) and livestock areas (90 million animals,

336   data was available at the website http://faostat3.fao.org) in Southeast Asia might promote

337   the enrichment of amine particles. Note that after the activation of amine particles, the

338   partitioning of the gas amine on cloud droplets may further contribute to the enhanced

339   Amine cloud residues (Rehbein et al., 2011), especially for air masses delivered via routes

340   with high relative humidity, as mentioned above (Figure S4). In contrast, northerly air mass

341   accompanied with dry airstreams may inadequately induce the partitioning of gas amines

342   into the particle phase (Rehbein et al., 2011).

343

344   **3.5 Comparison of cloud residues with ambient and interstitial particles**

345   A direct comparison between cloud residues and ambient particles was limited because of

346   their differences in air mass origins. During the sampling period, the cloud events occurred

347   once the southwesterly air masses were dominant. Therefore, a comparison between cloud

348   residues and ambient particles cannot be addressed under the influence of southwesterly

349   air masses. Here, we chose five hours before and after the beginning of the cloud II period

350   in order to compare cloud residues and ambient particles with similar northerly air mass

351   origins, as discussed in Sect 3.4. The time, detected number and Nf of ambient particles

352   for this comparison are listed in Table 1. From 10:00 21 January to 13:00 23 January, the

353   particles were manually switched in an hourly cycle between the CVI and ambient inlets

354   during the cloud III period to provide information on cloud residues and interstitial particles.

355   The number and Nf of particle types in the cloud residues and interstitial particles are given

356   in Table 2. Note that air mass origin shifted from southwesterly to northerly during 22-23

357   January.

358   Table 1 shows that the contribution of K-rich particles in cloud residues slightly

359   decreased relative to ambient particles (23.9% versus 30.7%), which may be due to the

360   small size distribution of K-rich in ambient particles (Figure S5). A slight increase in the

361   aged EC cloud residues was attributed to the decreased K-rich cloud residues. The

362   remaining particle types showed no clear differences between cloud residues and ambient

363   particles. A comparison of cloud residues and ambient particles may yield information on

364   particle's CCN activity due to the in-cloud processing effect. Rather, differences between

365   cloud residues and interstitial particles can better reflect whether particles become activated

366   (Zelenyuk et al., 2010). However, few studies have focused on this issue, in part because

367   interstitial particles show a smaller size than that detected by single-particle mass

368   spectrometry (Roth et al., 2016). In comparing the cloud residues with the interstitial

369   particles, a significant change in Nf was found for the aged EC and K-rich type. A higher

370   Nf of K-rich particles and a lower Nf of EC particles were found for the cloud residues

371   relative to the interstitial particles (Table 2). Aged EC particles may require very high

372   supersaturation to grow into cloud droplets and thus only form interstitial hydrated aerosol

373   (Hallberg et al., 1994).

374   Nitrate intensity was found to be enhanced for the cloud residues relative to the ambient

375   particles, as shown in Figure 7. Drewnick et al. (2007) suggested that, high nitrate, rather

376   than sulfate, content in pre-existing particles preferentially acted as cloud droplets. Hayden

377   et al. (2008) argued that a high nitrate content in cloud residues resulted from the uptake

378   of HNO_3 gas during the cloud process and estimated that the absorption of HNO_3 gas has

379   the increment of 100-200 nm nitrate cloud residues. However, this is not likely to be the

380   dominant source of 300-500 nm nitrate cloud residues in this study (Figure S6). The

381   enhancement of nitrate in cloud residues may be explained by pre-existing particles before

382   activation, rather than in-cloud nitrate formation. Interestingly, we observed a decrease in

383   nitrate intensity in cloud residues (Figure 8) and a large size distribution of nitrate-

384   containing cloud residues compared with the interstitial particles (Figure S7). This result

385   suggests that particle size, rather than nitrate content, plays a more important role in the

386   activation of particles into cloud droplets.

387   Sulfate intensity increased for the aged EC and OC cloud residues, while it decreased

388   for the Dust, Na-rich cloud residues compared with both ambient and interstitial particles.

389   Although the in-cloud addition of sulfate occurred by an aqueous Fe-catalyzed reaction

390   (Harris et al., 2013), sulfate was observed to diminish in the Fe cloud residues relative to

391   ambient particles. Compared with interstitial particles, sulfate enhanced in the Fe cloud

392   residues. In a similar comparison of cloud residues with interstitial particles, ambient

393   particles were observed for the K-rich type. Previous studies also showed that the mass or

394   number fraction of sulfate in the cloud residues changed between ambient and interstitial

395   particles (Pratt et al., 2010a; Hao et al., 2013; Schneider et al., 2016). However, the reason

396   for this discrepancy remains unclear.

397   No remarkable change in organic signals between cloud residues and ambient interstitial

398   particles was obtained for the different particle types. The in-cloud process was an

399   important pathway for the production of amine particles (Rehbein et al., 2011; Zhang et al.,

400   2012a). In this study, no significant enhancement of the Amine cloud residues was obtained

401   relative to the ambient particles (Table 1). Bi et al. (2016) considered that the absence of

402   amine species in fog residues may be partially affected by droplet evaporation in the GCVI.

403   We did find a high fraction of the Amine cloud residues when the southwesterly air mass

404   prevailed, as discussed in Sect 3.4. Therefore, the effect of amine volatilization in the GCVI

405   on the reduction of the Amine cloud residues is likely an unimportant factor in this study.

406   A lack of gas-phase amines may be the cause of few amine particles detected in the ambient

407   particles and cloud residues (Rehbein et al., 2011).

408

409   **3.6 Comparison with previous studies on cloud/fog residues**

410   Our finding can be compared with previous observations of cloud residues in various

411   environments including mountain sites (Kamphus et al., 2010; Roth et al., 2016) and

412   aircraft measurement (Zelenyuk et al., 2010). In these studies, cloud residues showed a

413   larger size distribution relative to ambient and/or interstitial particles, although in-cloud

414   processes may modify the size distribution of cloud residues. Cloud residues also exhibited

415   discrepancies in particle types. The aged EC particles in the stratocumulus cloud residues

416   were negligible at an altitude of 2-3 km over Alaska (Zelenyuk et al., 2010). In another

417   study, Pratt et al. (2010a) observed the abundant soot (~19% by number) and biomass

418   burning (~43% by number) mix-phase cloud residues at an altitude of 5-7 km over

419   Wyoming. High Nf of soot (~30%) and biomass burning (~25%) orographic cloud residues

420   were also observed at a mountain site Schmücke (937 m a.s.l.) in central Germany (Roth

421   et al., 2016). However, at Jungfraujoch station (3580 m a.s.l.) in Europe, the K-rich

422   (biomass burning) particles was only found to contribute 3% of the mix-phase cloud

423   droplets and the aged EC cloud residue was insignificant (< 1% by number) (Kamphus et

424   al., 2010). At a ground site in Guangzhou city, aged EC particles contributed up to 67.7%

425   of fog residues by number (Bi et al., 2016). In this study, aged EC and K-rich particles

426   dominated the cloud residues. We also found no distinct change in the Nf of aged EC and

427   K-rich particles in cloud residues relative to ambient particles, which was consistent with

428   the previous observation of the mix-phase cloud condition (Pratt et al., 2010a). However,

429   Roth et al. (2016) reported a higher Nf of aged soot particles in orographic cloud residues

430   rather than ambient particles, but no clear difference between cloud residues and ambient

431   particles for the biomass burning particle type. This disagreement between studies may

432   suggest that the ability of particle types to form cloud droplets strongly varies depending

433   on geographic location rather than cloud type and altitude.

434

435   **4 Conclusions**

436   This study presented an in situ observation of individual cloud residues, interstitials and

437   ambient particles at a mountain site in South China. We found that the largest fraction of

438   cloud residues was the aged EC type (49.3%), followed by K-rich particles (33.9%). The

439   remarkable change in Nf of the cloud residue types influenced by varied air masses

440   highlights the important role of regional transportation in the observed cloud residue

441 chemistry. Analysis of the mixing state of cloud residues showed that the Dust and Na-rich

442 cloud residues were highly associated with nitrate. We also conducted comparisons of

443 cloud residues with ambient and interstitial particles. Nitrate was found to be enhanced in

444 cloud residues relative to ambient particles but decreased relative to interstitial particles.

445 However, a larger size distribution of nitrate in the cloud residues was observed relative to

446 both ambient and interstitial particles. This difference suggests that the nucleating ability

447 of nitrate-containing particles to form cloud droplets is determined by the content and/or

448 size of nitrate. Sulfate increased in the aged EC and OC cloud residues while it decreased

449 in the Dust and Na-rich cloud residues compared with both ambient and interstitial particles.

450

451 **Acknowledgments**

452 The authors thank Ji Ou from Shaoguan city Environmental Monitoring Center for the

453 support at the observed site. We also acknowledge the NOAA Air Resources Laboratory

454 (ARL) for the provision of the HYSPLIT transport and dispersion model and/or READY

455 website (http://ready.arl.noaa.gov) used in this publication. This work was supported by

456 the National Nature Science Foundation of China (No. 91544101 and 41405131), the

457 "Strategic Priority Research Program (B)" of the CAS (XDB05020205), and the

458 Foundation for Leading Talents of the Guangdong Province Government. All the data can

459 be obtained by contacting the corresponding author.

460

References

Andreae, M. O., and Rosenfeld, D.: Aerosol-cloud-precipitation interactions. Part 1. The nature and sources of cloud-active aerosols, Earth-Sci. Revi., 89, 13-41, doi: 10.1016/j.earscirev.2008.03.001, 2008.

Angelino, S., Suess, D. T., and Prather, K. A.: Formation of aerosol particles from reactions of secondary and tertiary alkylamines: Characterization by aerosol time-of-flight mass spectrometry, Environ. Sci. Technol., 35, 3130-3138, doi: 10.1021/es0015444, 2001.

Bi, X., Dai, S., Zhang, G., Qiu, N., Li, M., Wang, X., Chen, D., Peng, P. a., Sheng, G., Fu, J., and Zhou, Z.: Real-time and single-particle volatility of elemental carbon-containing particles in the urban area of Pearl River Delta region, China, Atmos. Environ., 118, 194-202, doi: 10.1016/j.atmosenv.2015.08.012, 2015.

Bi, X., Lin, Q., Peng, L., Zhang, G., Wang, X., Brechtel, F. J., Chen, D., Li, M., Peng, P. a., Sheng, G., and Zhou, Z.: In situ detection of the chemistry of individual fog droplet residues in the Pearl River Delta region, China, J. Geophys. Res. Atmos., 121(15), 9105-9116, doi:10.1002/2016jd024886, 2016.

Berg, L.K., Berkowitz, C.M., Hubbe, J.M., Ogren, J.A., Hostetler, C.A., Ferrare, R.A., Hair, J.W., Dubey, M.K., Mazzoleni, C. and Andrews, E.: Overview of the cumulus humilis aerosol processing study. B. Am. Meteorol. Soc. 90, 1653-1667, http://dx.doi.org/10.1175/2009BAMS2760.1, 2009.

Bond, T. C., Doherty, S. J., Fahey, D. W., Forster, P. M., Berntsen, T., DeAngelo, B. J., Flanner, M. G., Ghan, S., Kärcher, B., Koch, D., Kinne, S., Kondo, Y., Quinn, P. K., Sarofim, M. C., Schultz, M. G., Schulz, M., Venkataraman, C., Zhang, H., Zhang, S., Bellouin, N., Guttikunda, S. K., Hopke, P. K., Jacobson, M. Z., Kaiser, J. W., Klimont,

484   Z., Lohmann, U., Schwarz, J. P., Shindell, D., Storelvmo, T., Warren, S. G., and Zender,

485   C. S.: Bounding the role of black carbon in the climate system: A scientific assessment,

486   J. Geophys. Res. Atmos., 118, 5380-5552, doi:10.1002/jgrd.50171, 2013.

487   Boucher, O., D. Randall, P. Artaxo, C. Bretherton, G. Feingold, P. Forster, V.-M.

488   Kerminen, Y. Kondo, H. Liao, U. Lohmann, P. Rasch, S.K. Satheesh, S. Sherwood, B.

489   Stevens and X.Y. Zhang: Clouds and Aerosols. In: Climate Change 2013: The Physical

490   Science Basis. Contribution of Working Group I to the Fifth Assessment Report of the

491   Intergovernmental Panel on Climate Change [Stocker, T.F., D. Qin, G.-K. Plattner, M.

492   Tignor, S.K. Allen, J. Boschung, A. Nauels, Y. Xia, V. Bex and P.M. Midgley (eds.)].

493   Cambridge University Press, Cambridge, United Kingdom and New York, NY, USA.

494   2013

495   Drewnick, F., Schneider, J., Hings, S. S., Hock, N., Noone, K., Targino, A., Weimer, S.,

496   and Borrmann, S.: Measurement of ambient, interstitial, and residual aerosol particles

497   on a mountaintop site in central Sweden using an aerosol mass spectrometer and a CVI,

498   J. Atmos. Chem., 56, 1-20, doi:10.1007/s10874-006-9036-8, 2007.

499   Deng X, Wu D, Shi Y, et al. Comprehensive analysis of the macro-and micro-physical

500   characteristics of dense fog in the area south of the Nanling Mountains (in Chinese),

501   J.Trop. Meteorol., 23(5): 424-434, 2007.

502   Duncan, B. N., Martin, R. V., Staudt, A. C., Yevich, R., & Logan, J. A.: Interannual and

503   seasonal variability of biomass burning emissions constrained by satellite observations,

504   J. Geophys. Res. Atmos., 108(D2), doi:108, 10.1029/2002jd002378, 2003.

505   Facchini, M. C., Decesari, S., Rinaldi, M., Carbone, C., Finessi, E., Mircea, M., Fuzzi, S.,

506   Moretti, F., Tagliavini, E., and Ceburnis, D.: Important source of marine secondary

507   organic aerosol from biogenic amines, Environ. Sci. Technol., 42, 9116-9121, doi:

508   10.1021/es8018385, 2008.

509   Furukawa, T., and Takahashi, Y.: Oxalate metal complexes in aerosol particles:

510   implications for the hygroscopicity of oxalate-containing particles, Atmos. Chem. Phys.,

511   11, 4289-4301, doi:10.5194/acp-11-4289-2011, 2011.

512   Hallberg, A., Ogren, J. A., Noone, K. J., Okada, K., Heintzenberg, J., & Svenningsson, I.

513   B.: The influence of aerosol particle composition on cloud droplet formation, J. Atmos.

514   Chem., 19, 153-171, doi: 10.1007/978-94-011-0313-8_8,1994.

515   Hao, L., Romakkaniemi, S., Kortelainen, A., Jaatinen, A., Portin, H., Miettinen, P.,

516   Komppula, M., Leskinen, A., Virtanen, A., Smith, J. N., Sueper, D., Worsnop, D. R.,

517   Lehtinen, K. E., and Laaksonen, A.: Aerosol chemical composition in cloud events by

518   high resolution time-of-flight aerosol mass spectrometry, Environ. Sci. Technol., 47,

519   2645-2653, doi:10.1021/es302889w, 2013.

520   Harris, E., Sinha, B., van Pinxteren, D., Tilgner, A., Fomba, K. W., Schneider, J., Roth, A.,

521   Gnauk, T., Fahlbusch, B., and Mertes, S.: Enhanced role of transition metal ion catalysis

522   during in-cloud oxidation of SO_2, Science, 340, 727-730, doi:10.1126/science.1230911,

523   2013.

524   Harris, E., Sinha, B., van Pinxteren, D., Schneider, J., Poulain, L., Collett, J., D'Anna, B.,

525   Fahlbusch, B., Foley, S., Fomba, K. W., George, C., Gnauk, T., Henning, S., Lee, T.,

526   Mertes, S., Roth, A., Stratmann, F., Borrmann, S., Hoppe, P., and Herrmann, H.: In-

527   cloud sulfate addition to single particles resolved with sulfur isotope analysis during

528   HCCT-2010, Atmos. Chem. Phys., 14, 4219-4235, doi:10.5194/acp-14-4219-2014,

529   2014.

530 Hayden, K. L., Macdonald, A. M., Gong, W., Toom-Sauntry, D., Anlauf, K. G., Leithead,

531   A., Li, S. M., Leaitch, W. R., and Noone, K.: Cloud processing of nitrate, J. Geophys.

532   Res. Atmos., 113(D18), doi:10.1029/2007jd009732, 2008.

533 Herich, H., Kammermann, L., Gysel, M., Weingartner, E., Baltensperger, U., Lohmann,

534   U., and Cziczo, D. J.: In situ determination of atmospheric aerosol composition as a

535   function of hygroscopic growth, J. Geophys. Res. Atmos., 113(D16),

536   doi:10.1029/2008jd009954, 2008.

537 Kamphus, M., Ettner-Mahl, M., Klimach, T., Drewnick, F., Keller, L., Cziczo, D. J.,

538   Mertes, S., Borrmann, S., and Curtius, J.: Chemical composition of ambient aerosol, ice

539   residues and cloud droplet residues in mixed-phase clouds: single particle analysis

540   during the Cloud and Aerosol Characterization Experiment (CLACE 6), Atmos. Chem.

541   Phys., 10, 8077-8095, doi:10.5194/acp-10-8077-2010, 2010.

542 Lee, C. S. L., Li, X., Zhang, G., Peng, X., and Zhang, L.: Biomonitoring of trace metals in

543   the atmosphere using moss (Hypnum plumaeforme) in the Nanling Mountains and the

544   Pearl River Delta, Southern China. Atmos. Environ., 39(3), 397-407, 2005.

545 Li, L., Huang, Z., Dong, J., Li, M., Gao, W., Nian, H., Fu, Z., Zhang, G., Bi, X., and Cheng,

546   P.: Real time bipolar time-of-flight mass spectrometer for analyzing single aerosol

547   particles, Int. J. Mass Spectrom., 303, 118-124,

548   doi:http://dx.doi.org/10.1016/j.ijms.2011.01.017, 2011.

549 Li, W., and Shao, L.: Observation of nitrate coatings on atmospheric mineral dust particles,

550   Atmos. Chem. Phys., 9, 1863-1871, doi:10.5194/acp-9-1863-2009, 2009.

551 McFiggans, G., Artaxo, P., Baltensperger, U., Coe, H., Facchini, M. C., Feingold, G., Fuzzi,

552   S., Gysel, M., Laaksonen, A., and Lohmann, U.: The effect of physical and chemical

553   aerosol properties on warm cloud droplet activation, Atmos. Chem. Phys., 6, 2593-2649,

554   doi:10.5194/acp-6-2593-2006, 2006.

555   Moffet, R., Foy, B. d., Molina, L. a., Molina, M., and Prather, K.: Measurement of ambient

556   aerosols in northern Mexico City by single particle mass spectrometry, Atmos. Chem.

557   Phys., 8, 4499-4516, doi:10.5194/acp-8-4499-2008, 2008.

558   Prabhakar, G., Ervens, B., Wang, Z., Maudlin, L. C., Coggon, M. M., Jonsson, H. H.,

559   Seinfeld, J. H., and Sorooshian, A.: Sources of nitrate in stratocumulus cloud water:

560   Airborne measurements during the 2011 E-PEACE and 2013 NiCE studies, Atmos.

561   Environ., 97, 166-173, doi:10.1016/j.atmosenv.2014.08.019, 2014.

562   Pratt, K. A., Hatch, L. E., and Prather, K. A.: Seasonal volatility dependence of ambient

563   particle phase amines, Environ. Sci. Technol., 43, 5276-5281, doi:10.1021/es803189n,

564   2009.

565   Pratt, K. A., Heymsfield, A. J., Twohy, C. H., Murphy, S. M., DeMott, P. J., Hudson, J. G.,

566   Subramanian, R., Wang, Z., Seinfeld, J. H., and Prather, K. A.: In Situ Chemical

567   Characterization of Aged Biomass-Burning Aerosols Impacting Cold Wave Clouds, J.

568   Atmos. Sci., 67, 2451-2468, doi:10.1175/2010jas3330.1, 2010a.

569   Pratt, K. A., and Prather, K. A.: Aircraft measurements of vertical profiles of aerosol

570   mixing states, J. Geophys. Res. Atmos., 115(D11), doi: 10.1029/2009jd013150, 2010.

571   Pratt, K. A., Twohy, C. H., Murphy, S. M., Moffet, R. C., Heymsfield, A. J., Gaston, C. J.,

572   DeMott, P. J., Field, P. R., Henn, T. R., Rogers, D. C., Gilles, M. K., Seinfeld, J. H., and

573   Prather, K. A.: Observation of playa salts as nuclei in orographic wave clouds, J.

574   Geophys. Res. Atmos., 115(D15), doi:10.1029/2009JD013606, 2010b.

575   Rehbein, P. J., Jeong, C. H., McGuire, M. L., Yao, X., Corbin, J. C., and Evans, G. J.:

576   Cloud and fog processing enhanced gas-to-particle partitioning of trimethylamine,

577   Environ. Sci. Technol., 45, 4346-4352, doi:10.1021/es1042113, 2011.

578   Roth, A., Schneider, J., Klimach, T., Mertes, S., van Pinxteren, D., Herrmann, H., and

579   Borrmann, S.: Aerosol properties, source identification, and cloud processing in

580   orographic clouds measured by single particle mass spectrometry on a central European

581   mountain site during HCCT-2010, Atmos. Chem. Phys., 16, 505-524, doi:10.5194/acp-

582   16-505-2016, 2016.

583   Schneider, J., Mertes, S., van Pinxteren, D., Herrmann, H., and Borrmann, S.: Uptake of

584   nitric acid, ammonia, and organics in orographic clouds: Mass spectrometric analyses of

585   droplet residual and interstitial aerosol particles, Atmos. Chem. Phys. Discuss., 1-38,

586   doi:10.5194/acp-2016-835, 2016.

587   Sellegri, K., Laj, P., Marinoni, A., Dupuy, R., Legrand, M., and Preunkert, S.: Contribution

588   of gaseous and particulate species to droplet solute composition at the Puy de Dôme,

589   France, Atmos. Chem. Phys., 3, 1509-1522, doi:10.5194/acp-3-1509-2003, 2003.

590   Shingler, T., Dey, S., Sorooshian, A., Brechtel, F. J., Wang, Z., Metcalf, A., Coggon, M.,

591   Mülmenstädt, J., Russell, L. M., Jonsson, H. H., and Seinfeld, J. H.: Characterisation and

592   airborne deployment of a new counterflow virtual impactor inlet, Atmos. Meas. Tech.,

593   5, 1259-1269, doi:10.5194/amt-5-1259-2012, 2012.

594   Song, X.H., Hopke, P. K., Fergenson, D. P., and Prather, K. A.: Classification of single

595   particles analyzed by ATOFMS using an artificial neural network, ART-2A, Anal.

596   Chem., 71, 860-865, doi:10.1021/ac9809682, 1999.

597   Sorooshian, A., Lu, M.-L., Brechtel, F. J., Jonsson, H., Feingold, G., Flagan, R. C., and

598   Seinfeld, J. H.: On the source of organic acid aerosol layers above clouds, Environ. Sci.

599   Technol., 41, 4647-4654, doi: 10.1021/es0630442, 2007a.

600   Sorooshian, A., Ng, N. L., Chan, A. W. H., Feingold, G., Flagan, R. C., and Seinfeld, J. H.:

601   Particulate organic acids and overall water-soluble aerosol composition measurements

602   from the 2006 Gulf of Mexico Atmospheric Composition and Climate Study

603   (GoMACCS), J. Geophys. Res. Atmos., 112(D13), doi:10.1029/2007JD008537, 2007b.

604   Sorooshian, A., Murphy, S., Hersey, S., Gates, H., Padro, L., Nenes, A., Brechtel, F.,

605   Jonsson, H., Flagan, R., and Seinfeld, J.: Comprehensive airborne characterization of

606   aerosol from a major bovine source, Atmos. Chem. Phys., 8, 5489-5520, doi:

607   http://dx.doi.org/10.5194/acp-8-5489-2008, 2008.

608   Tang, M., Cziczo, D. J., and Grassian, V. H.: Interactions of Water with Mineral Dust

609   Aerosol: Water Adsorption, Hygroscopicity, Cloud Condensation, and Ice Nucleation,

610   Chem. Rev., doi:10.1021/acs.chemrev.5b00529, 2016.

611   Twohy C.H. and Anderson J. R.: Droplet nuclei in non-precipitating clouds: composition

612   and size matter. Environ. Res. Lett., 3, 045002, doi:10.1088/1748-9326/3/4/045002,

613   2008.

614   Wang, Y., Guo, J., Wang, T., Ding, A., Gao, J., Zhou, Y., Collett, J. L., and Wang, W.:

615   Influence of regional pollution and sandstorms on the chemical composition of cloud/fog

616   at the summit of Mt. Taishan in northern China, Atmos. Res., 99, 434-442,

617   doi:10.1016/j.atmosres.2010.11.010, 2011.

618   Wu, Z., Nowak, A., Poulain, L., Herrmann, H., and Wiedensohler, A.: Hygroscopic

619   behavior of atmospherically relevant water-soluble carboxylic salts and their influence

620   on the water uptake of ammonium sulfate, Atmos. Chem. Phys., 11, 12617-12626,

621   doi:10.5194/acp-11-12617-2011, 2011.

622 Zelenyuk, A., Imre, D., Earle, M., Easter, R., Korolev, A., Leaitch, R., Liu, P., Macdonald,

623   A. M., Ovchinnikov, M., and Strapp, W.: In Situ Characterization of Cloud

624   Condensation Nuclei, Interstitial, and Background Particles Using the Single Particle

625   Mass Spectrometer, SPLAT II†, Anal. Chem., 82, 7943-7951, doi:10.1021/ac1013892,

626   2010.

627 Zhang, Khalizov, A. F., Pagels, J., Zhang, D., Xue, H., and McMurry, P. H.: Variability in

628   morphology, hygroscopicity, and optical properties of soot aerosols during atmospheric

629   processing, P. N. A. S., 105, 10291-10296, doi:10.1073/pnas.0804860105, 2008.

630 Zhang, G., Bi, X., Chan, L. Y., Li, L., Wang, X., Feng, J., Sheng, G., Fu, J., Li, M., and

631   Zhou, Z.: Enhanced trimethylamine-containing particles during fog events detected by

632   single particle aerosol mass spectrometry in urban Guangzhou, China, Atmos. Environ.,

633   55, 121-126, doi:10.1016/j.atmosenv.2012.03.038, 2012a.

634 Zhang, G., Bi, X., Li, L., Chan, L. Y., Li, M., Wang, X., Sheng, G., Fu, J., and Zhou, Z.:

635   Mixing state of individual submicron carbon-containing particles during spring and fall

636   seasons in urban Guangzhou, China: a case study, Atmos. Chem. Phys., 13, 4723-4735,

637   doi:10.5194/acp-13-4723-2013, 2013.

638 Zhang, X., Wang, Y., Niu, T., Zhang, X., Gong, S., Zhang, Y., and Sun, J.: Atmospheric

639   aerosol compositions in China: spatial/temporal variability, chemical signature, regional

640   haze distribution and comparisons with global aerosols, Atmos. Chem. Phys., 12, 779-

641   799, doi:10.5194/acp-12-779-2012, 2012b.

642 Table 1. Time, sampled particles and number fraction of ambient particles and cloud residues during various air masses.

	Cloud residues (Southwesterly)		Cloud residues (Northerly)		Ambient particles (Northerly)	
Start	16-01-2016, 12:00; 21-01-2016, 00:00		18-01-2016, 20:20		18-01-2016, 15:00	
End	17-01-2016, 00:00; 22-01-2016, 00:00		19-01-2016, 01:00		18-01-2016, 20:00	
types	Total Number	Number fraction	Total Number	Number fraction	Total Number	Number fraction
Aged EC	423	0.237±0.011	2417	0.599±0.012	1491	0.538±0.014
K-rich	918	0.515±0.017	962	0.239±0.008	852	0.307±0.011
Amine	269	0.151±0.009	6	0.002±0.001	5	0.002±0.001
Dust	55	0.030±0.004	80	0.020±0.002	65	0.024±0.003
Fe	42	0.024±0.004	223	0.055±0.004	125	0.045±0.004
Pb	6	0.003±0.001	26	0.006±0.001	23	0.008±0.002
OC	17	0.010±0.002	184	0.046±0.003	111	0.040±0.004
Na-rich	42	0.024±0.004	134	0.033±0.003	98	0.035±0.004
Other	12	0.006±0.002	0	0.000	4	0.001±0.001
Total	1784	1.000	4032	1.000	2774	1.000

643

644 Table 2. Particle number and number fraction of cloud residues and interstitial particles
645 using a manually switched way during the cloud III period.

	Cloud residues		Interstitial particles	
Types	Total Number	Number fraction	Total Number	Number fraction
Aged EC	577	0.370±0.015	560	0.527±0.022
K-rich	775	0.497±0.019	308	0.290±0.017
Amine	81	0.052±0.006	1	0.001±0.001
Dust	21	0.013±0.003	38	0.036±0.006
Fe	39	0.025±0.004	45	0.041±0.006
Pb	4	0.003±0.001	6	0.006±0.002
OC	27	0.018±0.003	49	0.046±0.007
Na-rich	27	0.018±0.003	49	0.046±0.007
Other	7	0.004±0.002	7	0.007±0.002
Total	1558	1	1063	1

646
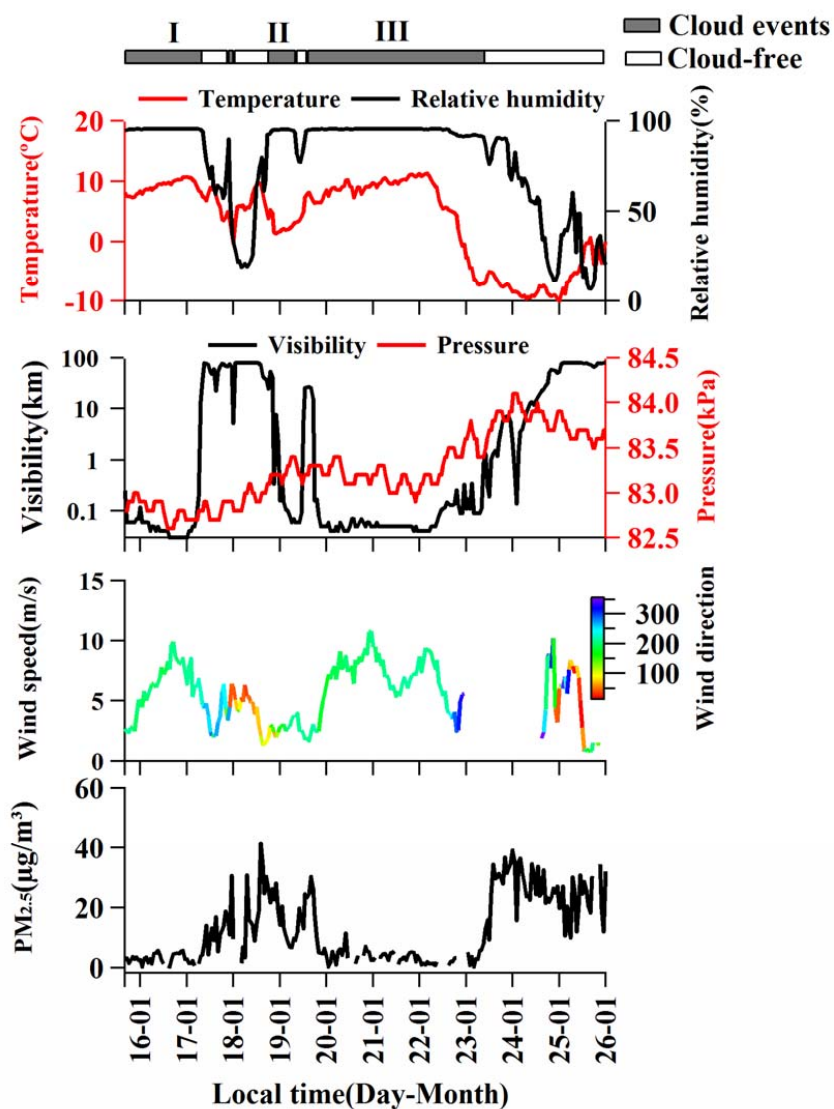
647

648   Figure 1: The hourly average variations in meteorological conditions (temperature, relative

649   humidity, visibility, pressure, wind speed and direction) and $PM_{2.5}$.
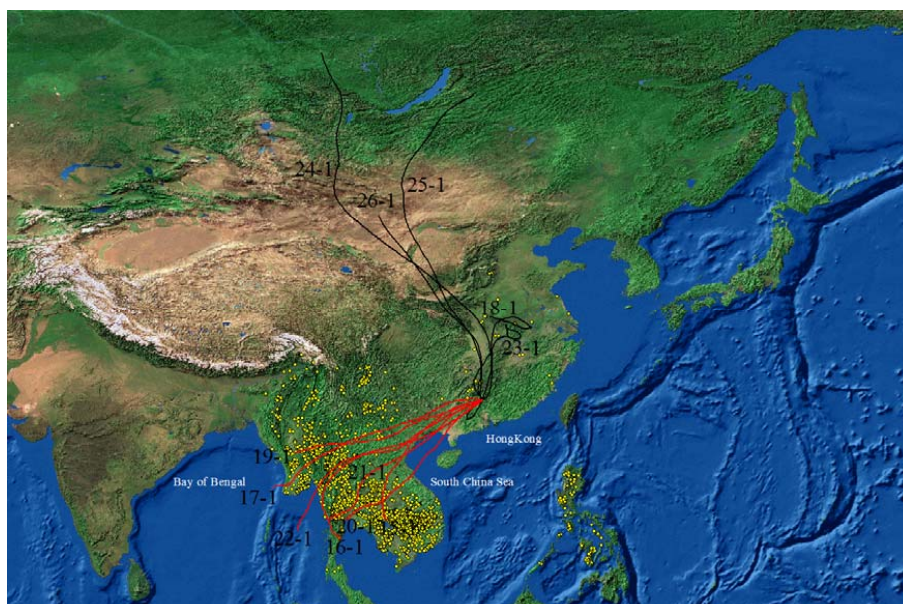
650
651
652   Figure 2: HYSPLIT back trajectories (72 h) for air masses at 1,800 m during the whole

653   sampling period. The black and red lines refer to northerly and southwesterly air masses,

654   respectively. The yellow rots represented the fire dots during the study periods. The fire

655   dots are available at https://earthdata.nasa.gov/.
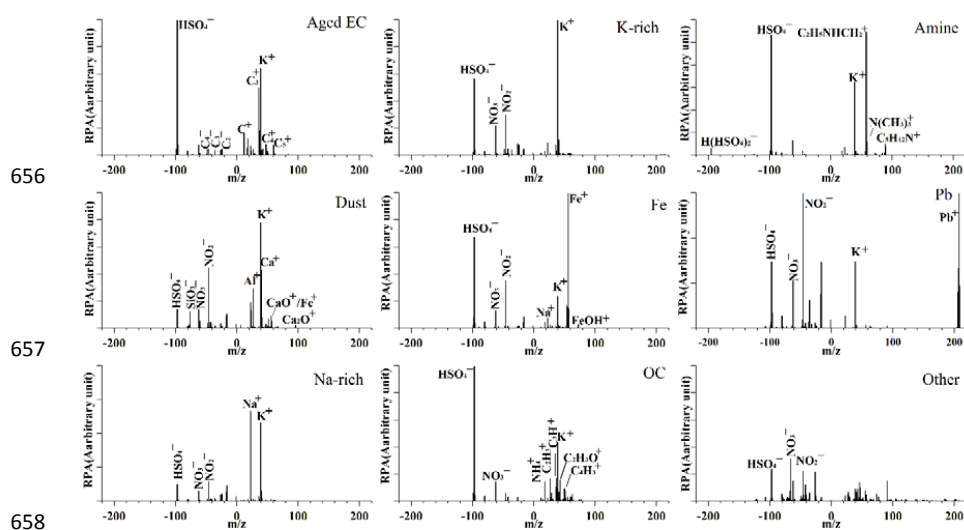
656

657

658
659

660   Figure 3: Averaged positive and negative mass spectra for the 9 particle types (Aged EC,

661   K-rich, Amine, Dust, Fe, Pb, Na-rich, OC, and Other) of the 73996 sampled particles

662   during the whole sampling period. RPA in the vertical axis refers to relative peak area. m/z

663   in the horizontal axis represents mass-to-charge ratio.

664
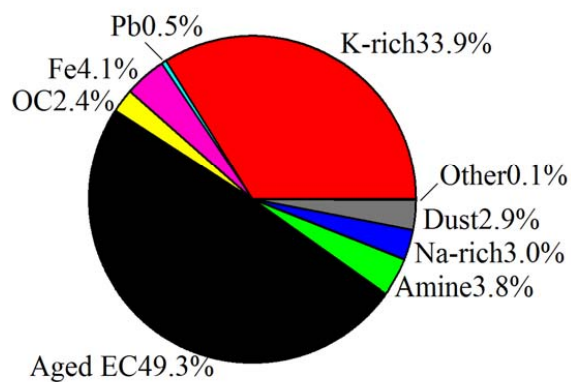
665
666   Figure 4: Number fraction of the cloud residual types during the whole sampling period.
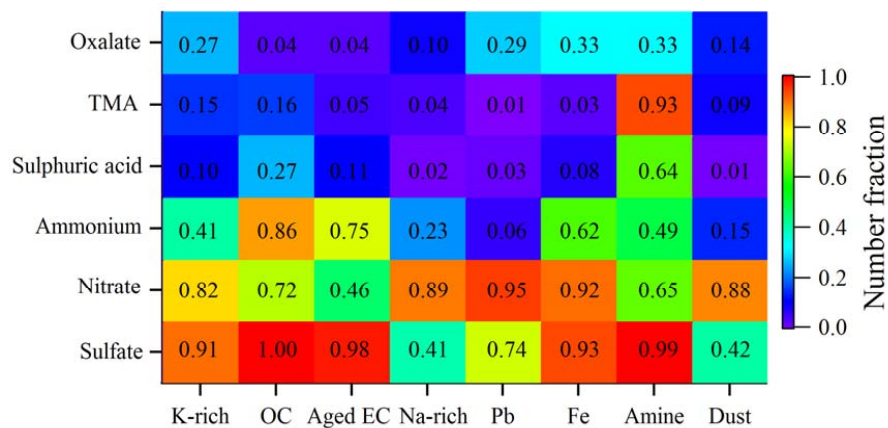
667
668
669   Figure 5: Mixing state of secondary markers with the cloud residue particle types.
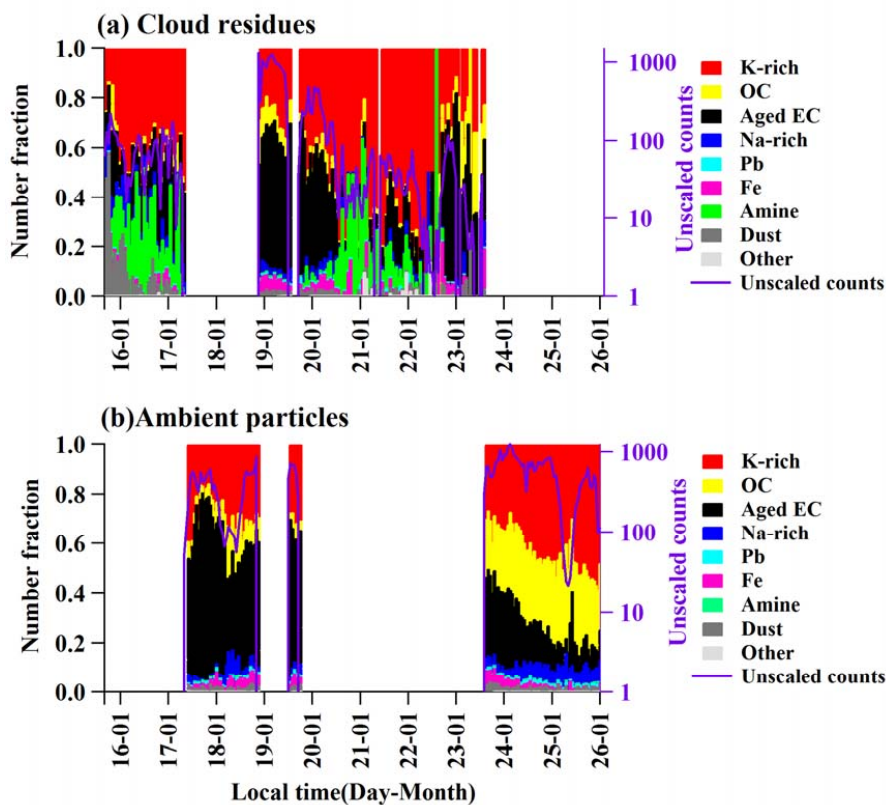
670

671
672   Figure 6: The hourly average variations in the cloud residual and ambient particles during

673   the whole sampling period.

674
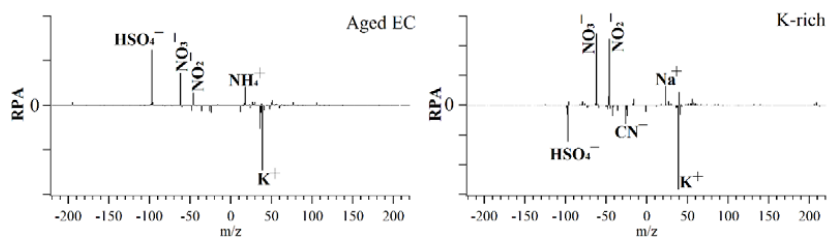
675
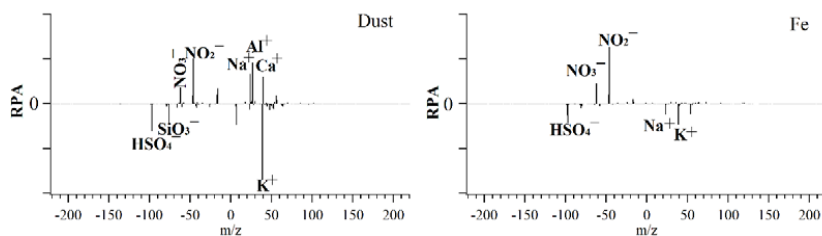
676
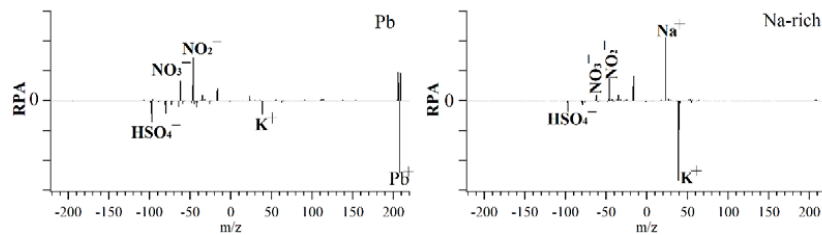
677
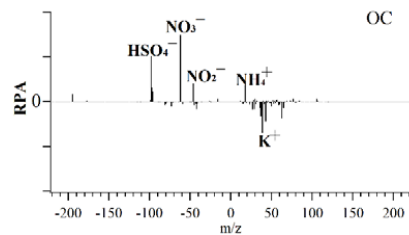
678
679

680   Figure 7: Difference between mass spectra for the cloud residues and ambient particles.

681

682

683
684
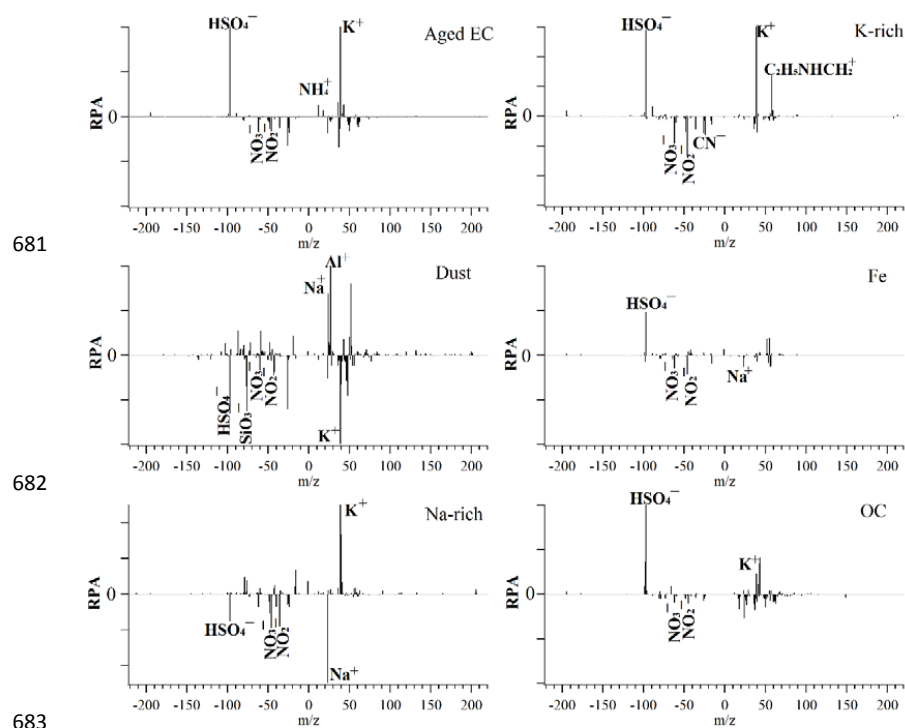
685   Figure 8: Difference between mass spectra for the cloud residues and interstitial particles.